Initial Dynamics of Cell Spreading Are Governed by Dissipation in the Actin Cortex

Jocelyn Étienne[†] and Alain Duperray[‡§]

[†]Laboratoire Interdisciplinaire de Physique, Université J. Fourier-CNRS, Saint Martin d'Hères, France; [‡]INSERM, U823, Grenoble, France; and [§]Université Joseph Fourier-Grenoble I, Faculté de Médecine, Institut d'oncologie et du développement Albert Bonniot, UMR-S823, Grenoble, France

SUPPLEMENTARY MATERIAL

Legend to Supplementary Movie 1

Time-lapse animation corresponding to Fig. 1a. The white contour in Fig. 1a is shown in blue in the movie. It corresponds to a fluorescence-intensity threshold which is taken at a fixed value throughout the duration of the movie. Note the transient nature of protrusions outside the blue contour.

Modelling and numerical technique

Modelling live cells is a formidable entreprise which is still far out of reach. However, in situations such as the initial spreading of cells, experimental results give some hope that only a few of the features of the living cell are setting the dynamics, which may allow for a simple model to explain them. Thus we proceed by introducing the simplest possible model for this precise situation and gradually introducing features until a behaviour similar to the one observed in cells is obtained, and is robust to parameter variations.

Cells in suspension are very much spherical but they are strongly inhomogeneous in their composition. The central part (around 10% to 20% volume, or 50% radius) is occupied by a nucleus. Around the nucleus is the cytoplasm, a porous medium composed of polymerised, reticulated proteins (the cytoskeleton), membrane-bound compartments of sub-micrometric size (organelles) and a fluid (the cytosol). The mechanical properties of the cytoplasm are expected to arise from the fluid (incompressibility, viscosity) and the cytoskeleton (elasticity or viscoelasticity, active remodelling fuelled by chemical energy). Mechanical response is dominated by a viscous-type response at shear rates lower than $0.1\,\mathrm{s}^{-1}$ (1) this can be understood because of the short lifetime of the reticulations and of the protein filaments themselves (order 1 s, see e.g. 2). The cytoskeleton is far from having a homogeneous distribution in the cell. Microtubules are highly rigid filaments arranged in a star-like manner from the centre of the cell to its periphery. For geometric reasons, they are not expected to sustain much stress during initial spreading. Actin filaments are concentrated in a cortex in the periphery of the cell (thickness of order 1 μm, (1)). Thus one can expect a higher viscosity in this outer region. The cell is enclosed by a membrane, which is bound to the actin cortex. The membrane is a lipid bilayer which prevents large molecules to enter the cell and creates osmotic effects. It is fluid (in-plane shear viscosity is low) and (nearly) inextensible. This inextensibility constraint is modulated by the presence of membrane "reservoirs" (either ruffles or invaginations). From frustrated spreading experiments by (3), where spreading is limited because only a small circular patch is functionalized and thus permits adhesion, we know that this readily accessible area is sufficient for the spread area to reach at least 700 $\mu\mathrm{m}^2$. This is large compared to the range of spread area considered in initial spreading, however the recruitment of these extra area reservoirs, located everywhere around the cell, may affect the spreading dynamics. Membrane area is then modulated by coalescence (and decoalescence) of small vesicles. This is an active biological process called exocytosis/endocytosis, happening on the time scale of 100 s (4). We do not directly consider this in our model, however as long as one assumes

that this process is not geometrically directed, its effects are similar to the presence of excess area.

Given the experimental observations, Stokes equations are expected to be a fair first-order approximation of the dissipative mechanisms in the dynamical process. Assuming that a lubrication layer thick of order $0.1\,\mu\mathrm{m}$ remains between cell and substrate, the shear rate is of order $1\ \mathrm{s}^{-1}$ initially and decreases, and the Reynolds number is vanishingly small. In the cell, a typical distance is $1\ \mu\mathrm{m}$ (the thickness of the shell of actin around the cell), so the shear rate is one order of magnitude lower. This means also that viscoelastic properties of the proteins in the cell cytoplasm will be dominated by viscous response. Buoyancy effects are sufficient to make cells sediment, however they are too weak to deform cells and, when cells are close enough to the substrate, they become negligible with respect to the adhesion force which then provides the only first order driving force. This adhesion force, in our case, may result either from specific or nonspecific interactions, without modifying the scaling laws of spreading. Thus we choose the simplest model we can think of, that is, a van der Waals-type potential of magnitude w, as proposed by (5) for nonspecific adhesion :

$$W(z) = w\left(\left(\frac{d_0^2}{z^2} - 1\right)^2 - 1\right). \tag{1}$$

We take the equilibrium distance of the potential $d_0 = 0.05R_0$ in this model for simulations, the invariance of the spreading profile (up to a scaling factor in time) has been checked with $d_0 = 0.01R_0$ in some cases.

We consider a cylindrical flow domain of symmetry axis $(O,\, \boldsymbol{e}_z)$, and denoted $\Omega \times [0,\, 2\pi]$ (using cylindrical coordinates, Fig. S1). This domain contains an incompressible Newtonian fluid of homogeneous viscosity $\eta = \eta_\mathrm{s}$ except in the drop or vesicle, which occupies a subdomain $\Omega_\mathrm{d}(t) \times [0,\, 2\pi]$ which is advected by the fluid velocity $\boldsymbol{u}$, and where viscosity η is equal to some function $\eta_\mathrm{d}(\boldsymbol{x}, t)$, also advected by the fluid velocity. This writes as:

$$\Omega_\mathrm{d}(t) = \{\boldsymbol{X}(\boldsymbol{x}_0, t), \boldsymbol{x}_0 \in \Omega_\mathrm{d}(t_0)\} \qquad \eta_\mathrm{d}(\boldsymbol{X}(\boldsymbol{x}_0, t), t) = \eta_\mathrm{d}(\boldsymbol{x}_0, t_0) \tag{2}$$

with $t \mapsto \boldsymbol{X}(\boldsymbol{x}_0, t)$ the trajectory of a material point occupying $\boldsymbol{x}_0$ at time t_0, defined by the Cauchy problem:

$$\begin{cases} \dfrac{\partial \boldsymbol{X}}{\partial t}(\boldsymbol{x}_0, t) &= \boldsymbol{u} \circ \boldsymbol{X}(\boldsymbol{x}_0, t), \quad t \in [0, T], \\ \boldsymbol{X}(\boldsymbol{x}_0, t_0) &= \boldsymbol{x}_0, \end{cases} \tag{3}$$

where $\boldsymbol{u} \circ \boldsymbol{X}(\boldsymbol{x}_0, t)$ is understood as $\boldsymbol{u}(\boldsymbol{X}(\boldsymbol{x}_0, t), t)$.

The structure of the problem should reflect our objective of describing a balance between adhesion force and viscous friction and be scale-invariant to a change in numerical value of any of the parameters. This is made clear by non-dimensionalising the problem by length R_0 (initial radius of the drop or vesicle), viscosity η_0 (largest viscosity in the problem), time $T = R_0\eta_0/w$ and pressure $P = w/R_0$, which does not introduce any nondimensional group in the governing equations:

$$-\mathrm{div}\ (2\eta\mathbb{D}(\boldsymbol{u})) + \boldsymbol{\nabla} p = 0 \qquad \text{in } \Omega \tag{4}$$

$$\mathrm{div}\, \boldsymbol{u} = 0 \qquad \text{in } \Omega \tag{5}$$

with boundary conditions (see Fig. S1):

$$\begin{aligned}
\boldsymbol{u} &= \mathbf{0} && \text{on } \Gamma_{\text{wall}},\\
u_r = 0, \qquad \frac{\partial u_z}{\partial r} &= 0 && \text{on } \Gamma_{\text{axis}},\\
-p\,\boldsymbol{n}_{\text{out}} + 2\eta\,\mathbb{D}(\boldsymbol{u})\,\boldsymbol{n}_{\text{out}} &= \mathbf{0} && \text{on } \Gamma_{\text{out}},\\
\left[-p\,\mathbb{I} + 2\eta\,\mathbb{D}(\boldsymbol{u})\right]_{\text{int}}\boldsymbol{n}_{\text{int}} &= -\boldsymbol{\nabla} W + \boldsymbol{f}_{\text{int}} && \text{on } \Gamma_{\text{int}}(t),
\end{aligned}$$

where $[\phi]_{\text{int}}$ denotes the jump of ϕ accross the interface $\Gamma_{\text{int}}(t)$, and $\boldsymbol{f}_{\text{int}}$ are interfacial forces other than the adhesion force $\boldsymbol{\nabla} W$.

For fluid drops suspended in a fluid in which they are immiscible, this force is equal to the capillary force. Since the dynamic balance we are looking for is between adhesion and viscous friction, we consider the limit of vanishing capillary tension (infinite capillary number), thus suppressing any competition between driving forces. This limit is relevant only in the first stages of drop spreading, which is the domain in which analogies between drop and cell spreading are investigated. At later stages, the behaviour of cells is driven by the complex machinery of its cytoskeleton (6), while for drops surface tension takes a leading order importance. Viscosity differs between the drop inside and medium, and is either supposed uniform within the cell or space dependent. Such models are called composite or compound drop models (7).

In some simulations it was desireable to explore the case of vanishing viscosity of the suspending medium (infinite viscosity contrast). The equations of the suspending fluid are then trivially reduced to a homogeneous pressure $p = 0$, and only the drop or vesicle is actually simulated.

Numerical simulations of membrane-bound drops (vesicles)

The cell membrane is a lipid bilayer, which is impermeable to large molecules but permeable to water. Although no accurate quantitative validation exist, it is generally assumed that at the time scale of a few hours permeability can be neglected; thus the membrane normal displacement is equal to the fluid normal displacement. Lipid bilayers are two-dimensional fluids, their in-plane shear viscosity is relatively small (8), but they are nearly incompressible (in their plane). This translates as an inextensible surface in the three-dimensional problem, inextensibility is enforced through a tension force, which has a tangential component equal to the gradient of tension (two-dimensional analogue of pressure). Bending this surface results in two distinct normal forces: bending rigidity, which originates from the dissymmetry of lipid layers introduced by curvature, and a normal component of the inextensibility force, which corresponds to the floppiness of the surface with respect to curvature reduction. In cells, the cytoskeleton underlying the plasmic membrane is bound to it at intervals (submicron scale) by transmembrane proteins and more densely by weaker lipid bonds (9). Thus the hydrodynamic boundary condition that applies on the flow of the cytoplasm is, to the first order, a no-slip condition on the membrane.

The interfacial forces correspond to the forces exerted by the membrane on the fluids. They originate from the bending rigidity, shear viscosity and inextensibility of

the membrane. For the same reason as for drops, we consider the limit of zero bending rigidity. Lipid bilayers have a low in-plane shear viscosity and, even for spectrin-lined membranes, has a negligible contribution to dynamics compared to bulk-viscosity in cells. (From the value of in-plane shear viscosity found by (8) for red blood cells, we expect dissipation in the eukaryotic cell membrane to be about 3 orders of magnitude smaller than in the bulk.) Inextensibility, however, is a constraint imposed to membrane flow and thus to fluid flow in its vicinity. It can be expressed in terms of the surface divergence of the (tangential) velocity along the membrane:

$$\operatorname{div}_\mathrm{s} \boldsymbol{u} = 0 \qquad\qquad \text{on } \Gamma(t), \tag{6}$$

Incompressibility and inextensibility constraints are much alike. We offer to treat them in the same framework of constrained minimisation. The Stokes problem above can be rewritten in terms of its energy. The solution $\boldsymbol{u}$ is such that

$$\begin{cases} J(\boldsymbol{u}) \leq J(\boldsymbol{v}) \quad \forall \boldsymbol{v}, \operatorname{div} \boldsymbol{v} = 0 \text{ in } \Omega(t) \text{ and } \operatorname{div}_\mathrm{s} \boldsymbol{v} = 0 \text{ on } \Gamma(t) \\ \operatorname{div} \boldsymbol{u} = 0 \text{ in } \Omega(t) \text{ and } \operatorname{div}_\mathrm{s} \boldsymbol{u} = 0 \text{ on } \Gamma(t) \end{cases} \tag{7}$$

(Surface divergence condition only applies to the case of membrane-bound vesicles.) Lagrange multipliers (pressure p and tension ζ) do not appear explicitely in this formulation. If we introduce them as test functions of the constraints,

$$\mathcal{L}(\boldsymbol{v};\, q, \xi) = J(\boldsymbol{v}) + \int_{\Omega(t)} q \operatorname{div} \boldsymbol{v} \,\mathrm{d}\boldsymbol{x} + \int_{\Gamma(t)} \xi \operatorname{div}_\mathrm{s} \boldsymbol{v} \,\mathrm{d}s, \tag{8}$$

then we can characterise the solution $\boldsymbol{u}$ in terms of an *unconstrained* minimisation problem:

$$\mathcal{L}(\boldsymbol{u};\, p, \zeta) = \min_{\boldsymbol{v}} \max_{q,\xi} \mathcal{L}(\boldsymbol{v}; q, \xi) \tag{9}$$

The Lagrange multiplier ζ is also completely characterised by this procedure as soon as the curvature is not everywhere zero. Pressure is defined up to a constant (so is tension if curvature is everywhere zero).

The energy landscape to be minimised is schematised in Fig. S2. Different methods can be used for this. Penalty methods consist in minimising the functional

$$J(\boldsymbol{v}) + r \int_{\Omega(t)} (\operatorname{div} \boldsymbol{v})^2 \,\mathrm{d}\boldsymbol{x} + r' \int_{\Gamma(t)} (\operatorname{div}_\mathrm{s} \boldsymbol{v})^2 \,\mathrm{d}s$$

where r and r' are penalty parameters : in order for the method to be exact, they need to be made to tend to the infinity, thus the minimum, initially located outside of the space such that $|\operatorname{div} \boldsymbol{v}| + |\operatorname{div}_\mathrm{s} \boldsymbol{v}| = 0$, converges to $\boldsymbol{u}$. It is however not practical to have r, r' too large. Projection methods minimise $J(\boldsymbol{v})$ globally and then project the result onto the space such that $|\operatorname{div} \boldsymbol{v}| + |\operatorname{div}_\mathrm{s} \boldsymbol{v}| = 0$, which introduces errors with respect to boundary conditions. Saddle-point methods, finally, consider the full problem in Eq. 9. One observes (sketch in Fig. S2) that the minimum of $\max_q \mathcal{L}(\boldsymbol{v};\, q)$ is exactly the point

described in Eq. 7. The augmented Lagrangian method (10) consists in adding to the Lagrange functional a penalty term:

$$\mathcal{L}_r(\boldsymbol{v}; q, \xi) = \mathcal{L}(\boldsymbol{v}; q, \xi) + r \int_{\Omega(t)} (\operatorname{div} \boldsymbol{v})^2 \, \mathrm{d}\boldsymbol{x} + r' \int_{\Gamma(t)} (\operatorname{div}_\mathrm{s} \boldsymbol{v})^2 \, \mathrm{d}s$$

One checks easily that saddle-points of $\mathcal{L}$ and $\mathcal{L}_r$ coincide for any choice of r, r', the latter however allows a faster convergence of iterative algorithms because non-divergence free velocity fields are penalised in minimisation steps (with respect to $\boldsymbol{v}$).

In order to represent the excess membrane area available prior to cell spreading (3), the numerical simulations of vesicles start from an initial condition where wrinkles are superimposed to the initial spherical shape (Fig. 5a).

In practice, the numerical simulations allow only for a limited scale separation between vesicle size and wrinkle size, since computational cost will grow with the number times the depth of wrinkles (and the depth of wrinkles roughly scales with their number for a given excess area). Therefore, we used 20 wrinkles of depth $0.05R_0$, rather than try to reproduce the very small scale membrane folds observed on real cells.

As the vesicle spreads, this geometry induces a step-like growth of aligned area, as bulges align very quickly with the substrate whereas dimples take some time to do so. For comparison with experiments, the growth of aligned area should not take these steps into account. In order to reduce the influence of these steps on the linear fits, we average first the spreading profile obtained in two calculations with wrinkles in spatial phase opposition (see Fig. S3).

Determination of the transition between linear and slow spreading regimes

The area of the aligned area is found to incur a growth close to linear in time until a time t^* (phase P_1). For $t > t^*$, the growth is much slower in time (phase P_2).

In order to determine automatically t^*, we calculate for each spreading experiment the least-square deviation $D_A(t) = \sum_{t_i<t} w_i (A(t_i) - Ct_i)^2$ of $A(t)$ with a linear curve Ct over the time lapse $[0, t]$, where w_i is a weight corresponding to the length of the interval, $w_i = \frac{1}{2}(t_{i+1} - t_{i-1})$, and C is an adjustable parameter minimizing $D_A(t)$ for $A(t) \leq 80\mu\mathrm{m}^2$, that is, before transition occurs in any spreading experiment. $D_A(t)$ is an increasing function of t, with a left-right inverted L-shape. t^* is then defined as the instant when $D_A(t^*)$ reaches $40\,000\mu\mathrm{m}^2\cdot\mathrm{s}$, meaning that $A(t)$ deviates strongly from linear increase for $t > t^*$. We define the transition area $A^* = A(t^*)$.

Numerical simulations

A finite element technique is employed to calculate an approximate solution of Eq. 7 for a sequence of times t_n, and $\Omega_d(t_{n+1})$ is obtained by advecting $\Omega_d(t_n)$ with the approximation of velocity $\boldsymbol{u}(t_n)$. This Lagrangian tracking of the interface is such that meshes of both the bulk and the interface coincide. Compared to methods where the bulk is meshed independently of the interface (such as level-set, phase-field and immersed boundary methods), the advantage is a greater accuracy due to the possibility of localising interfacial forces on the interface. Compared to boundary integral

methods, the advantage is versatility with respect to bulk-flow governing equations and geometry.

Lagrange multipliers and the velocity are calculated using a saddle-point approach (10, 11) with Uzawa algorithm. The residual was 10^{-12}. The method is implemented in the C++ open-source, free software `rheolef` (12).

The numerical method has been tested and validated with $O(h^{1.5})$ convergence against the analytical solution for drop oscillation modes of (13) (for the case of drops or composite drops) and the Stokes solution of the free fall of a spherical vesicle (11).

Determination of the aligned area in numerical simulations

The quantity of interest in simulations is the distance r from the symmetry axis over which interface $\Gamma_{\text{int}}(t)$ is close to $z = 0$ in some sense, which corresponds to the aligned area. We define the contact time as the instant from which the object starts to deform. We measure the aligned area by tracking from then the radial position of the point from which the interface $\Gamma_{\text{int}}(t)$ is 10^{-6} space units farther from the substrate than the closest point of the interface at the same instant. This procedure is relevant only to high viscosity contrasts, when the drainage of the lubrication film below the object is quick. For lower viscosity contrasts, we track the point from which the interface is above $z = d_0 + 0.02R_0$. At intermediate viscosity contrasts, these two definitions of the aligned area yield parallel curves with a small time lag.

In order to compare spreading profiles with power-laws $A = Ct^k$, best fit is calculated by least squares over the range $A = 1.6 \cdot 10^{-3}A_0$ to $A = 0.64A_0$. The upper bound corresponds to a lower estimate of the transition from phase P_1 to phase P_2 in experiments. The lower bound is a numerical cut-off. This cut-off is several times larger than the mesh size at the aligned area, because aligned area is not a primitive variable of the problem and needs to be evaluated by geometrical post-treatment. Error for the least squares ranges from 10^{-3} to $3 \cdot 10^{-2}$. These best-fit results for model objects and cells in experiments are shown in Fig. 6a as a function of the contrast of viscosity between the object and the suspending fluid.

Distribution of dissipation

In simulations, the only source of energy is the adhesion energy gained by spreading. Because there is no inertia or elasticity, all this energy is instantaneously dissipated by friction. Therefore, tracking dissipation and spread area is equivalent, and we obtain the same slopes in figures S5b, S6b and S7b as in figures 3d, 4d and 5d.

REFERENCES

1. F. Wottawah, S. Schinkinger, B. Lincoln, R. Ananthakrishnan, M. Romeyke, J. Guck, and J. Käs. Optical rheology of biological cells. *Phys. Rev. Lett.*, 94: 098103, 2005.

2. D.H. Wachsstock, W.H. Schwarz, and T.D. Pollard. Cross-linker dynamics determine the mechanical properties of actin gels. *Biophys. J.*, 66:801–809, 1994.

3. N. C. Gauthier, O. M. Rossier, A. Mathur, J. C. Hone, and M. P. Sheetz. Plasma membrane area increases with spread area by exocytosis of a gpi-anchored protein compartment. *Mol. Biol. Cell*, 20:3261–3272, 2009. doi: 10.1091/mbc.E09-01-0071.

4. M. P. Sheetz, J. E. Sable, and H.-G. Döbereiner. Continuous membrane-cytoskeleton adhesion requires continuous accommodation to lipid and cytoskeleton dynamics. *Annu. Rev. Biophys. Biomol. Struct.*, 35:417–434, 2006.

5. S. Sukumaran and U. Seifert. Influence of shear flow on vesicles near a wall: A numerical study. *Phys. Rev. E*, 64:011916, 2001.

6. I. Bischofs, F. Klein, D. Lehnert, M. Bastmeyer, and U. Schwarz. Filamentous network mechanics and active contractility determine cell and tissue shape. *Biophys. J.*, 95:3488–3496, 2008.

7. N. A. N'Dri, W. Shyy, and R. Tran-Son-Tay. Computational modeling of cell adhesion and movement using a continuum-kinetics approach. *Biophys. J.*, 85: 2273–2286, 2003.

8. R. Tran-Son-Tay, S. P. Sutera, and P. R. Rao. Determination of red blood cell membrane viscosity from rheoscopic observations of tank-treading motion. *Biophys. J.*, 46:65–72, 1984.

9. M. Sheetz. Cell control by membrane–cytoskeleton adhesion. *Nat. Rev. Mol. Cell Biol.*, 2:392–396, 2001.

10. M. Fortin and R. Glowinski. *Augmented Lagrangian methods, applications to the numerical solution of boundary value problems*. Elsevier Science, Amsterdam, 1983.

11. J. Étienne, J. Lohéac, and P. Saramito. A Lagrange-multiplier approach for the numerical simulation of an inextensible membrane or thread immersed in a fluid. Submitted, 2010. Preprint : `http://hal.inria.fr/inria-00449805/fr/`.

12. P. Saramito, N. Roquet, and J. Étienne. `rheolef`, a C++ finite element environment. Technical report, CNRS, 2003–2009. `http://www-lmc.imag.fr/lmc-edp/Pierre.Saramito/rheolef`.

13. A. Prosperetti. Free oscillations of drops and bubbles: the initial-value problem. *J. Fluid Mech.*, 100:333–347, 1980.

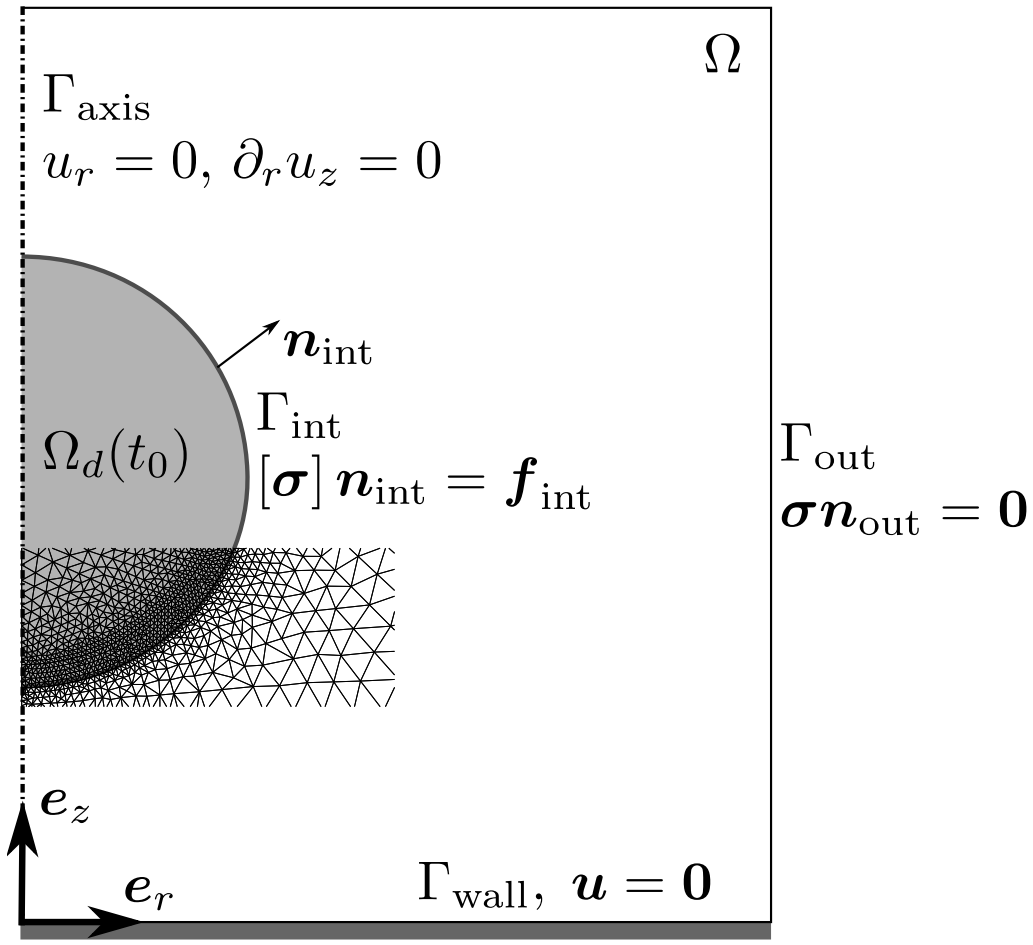

Figure S1: Computational domain and example of part of a finite element mesh used in numerical simulations.

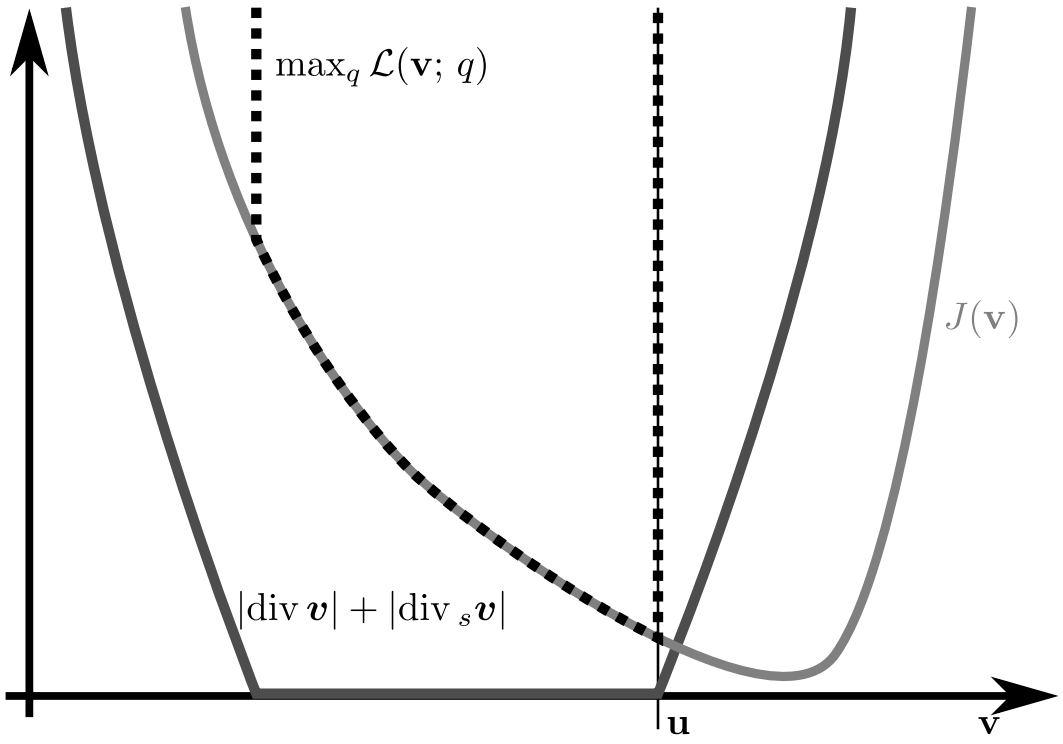

Figure S2: Sketch of the energy landscape of a constrained minimisation problem: functional $J(v)$ must be minimised under the condition that $|\mathrm{div}\, \boldsymbol{v}| + |\mathrm{div}_s\, \boldsymbol{v}| = 0$. Exact solution is $\boldsymbol{u}$, which is the minimum of $\max_q \mathcal{L}(\boldsymbol{v}; q)$.

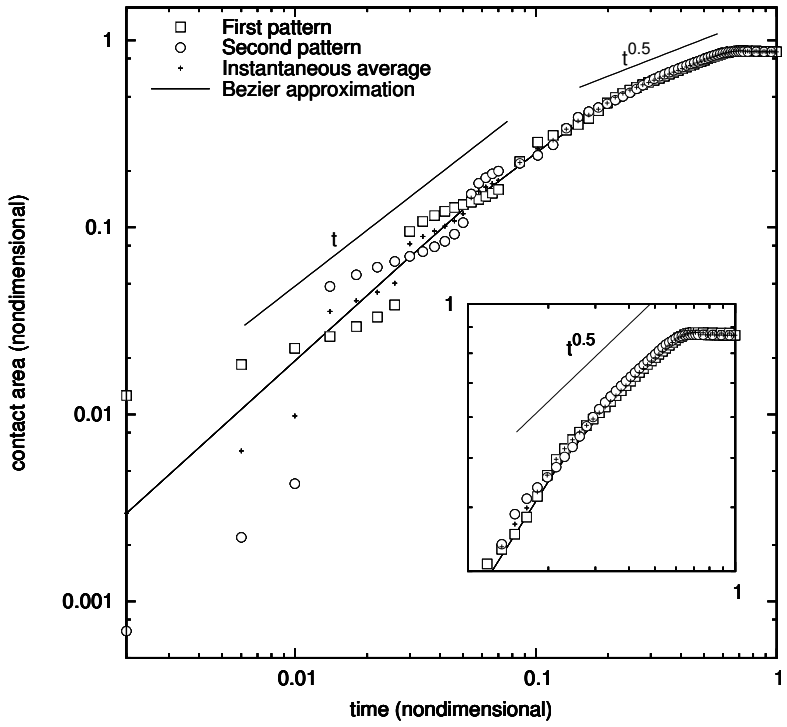

Figure S3: Growth of contact area of two vesicles with area reservoirs, viscosity contrast 100. Empty symbols represent vesicles, with wrinkle patterns in phase opposition. They exhibit step-like growth of aligned area due to their geometry. The instantaneous average of these values and their approximation with a Bézier curve partially smear out these steps and are easier to compare to power-laws.

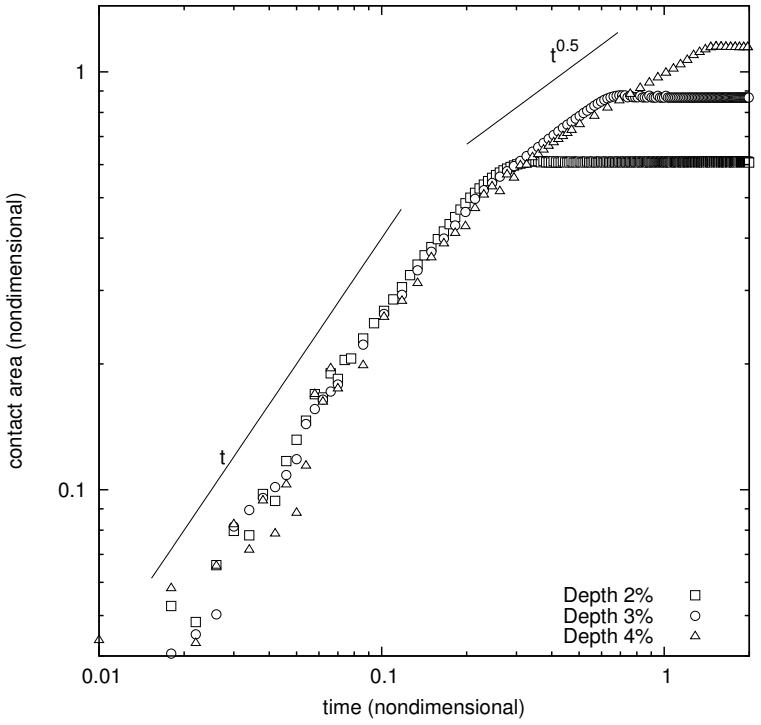

Figure S4: Growth of contact area of vesicles with area reservoirs of various depth, viscosity contrast 100.

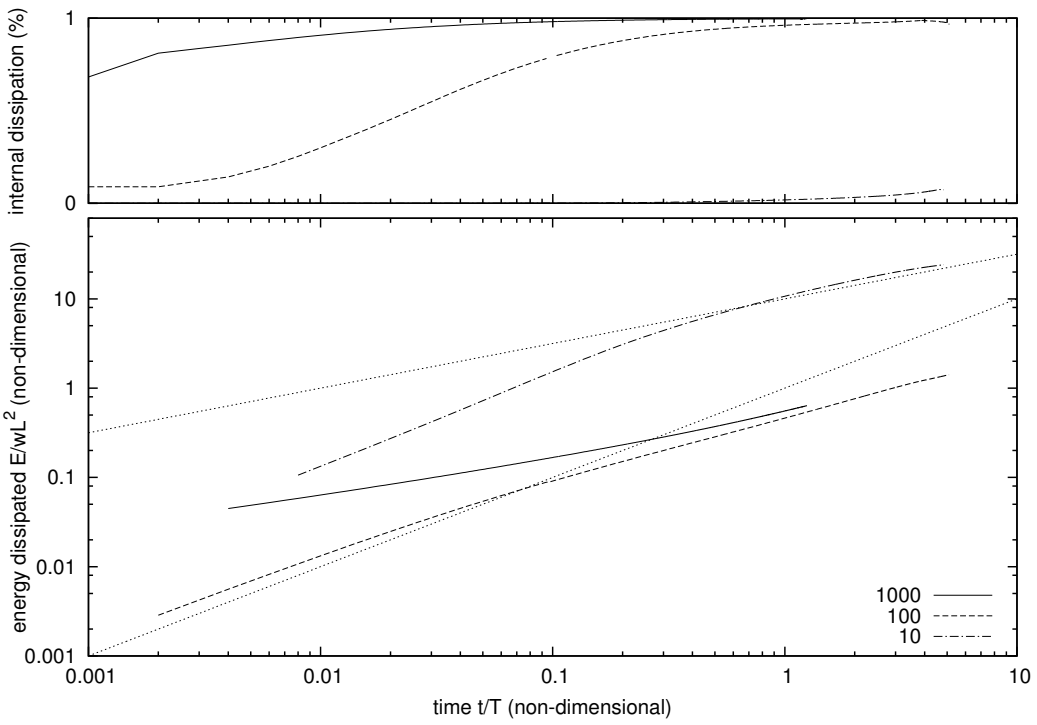

Figure S5: Dissipation as a function of time during initial drop spreading, for different viscosity ratios. (a), ratio of dissipation occuring inside the drop compared to total dissipation (medium included). (b), total dissipation incurred since the beginning of spreading.

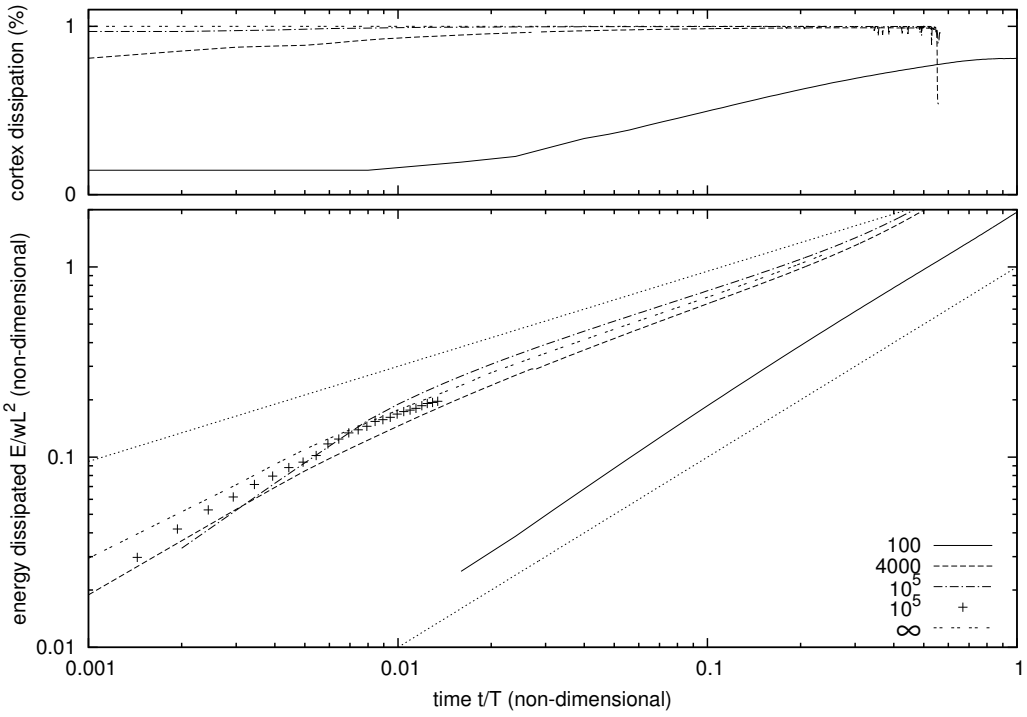

Figure S6: Dissipation as a function of time during initial spreading of a composite drop, for different viscosity ratios. (a), ratio of dissipation occuring inside the cortex compared to total dissipation (central, low-viscosity part and medium included). (b), total dissipation incurred since the beginning of spreading.

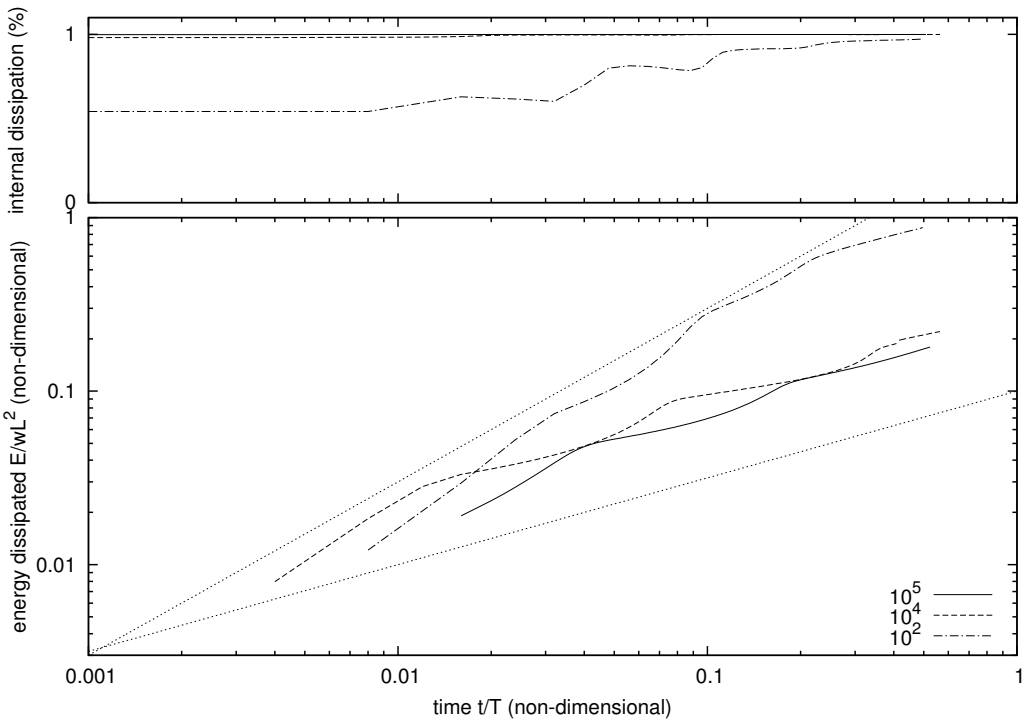

Figure S7: Dissipation as a function of time during initial spreading of a vesicle, for different viscosity ratios. (a), ratio of dissipation occuring inside the vesicle compared to total dissipation (medium included). (b), total dissipation incurred since the beginning of spreading.